processes

MDPI

Article

SFSO: Surrogate-Based Fluid Supply Optimization Method for Improving Efficiency and Pressure Stability in Longwall Hydraulic Systems

Tao Fu [1,2,3,*] and Rulin Zhou [1,2,4]

[1] State Key Laboratory of Digital Intelligent Technology for Unmanned Coal Mining, Beijing 101399, China
[2] Beijing Tianma Intelligent Control Technology Co., Ltd., Beijing 101399, China
[3] China Coal Research Institute, Beijing 100013, China
[4] School of Energy and Mining Engineering, China University of Mining and Technology-Beijing, Beijing 100083, China
* Correspondence: futao@alu.hit.edu.cn

Abstract

In longwall mining, conventional centralized fluid-supply systems generally operate at a fixed flow rate and therefore cannot respond effectively to the highly time-varying and overlapping demands of multiple hydraulic supports operating in coordination with an automated shearer. This mismatch can cause excessive relief flow, insufficient supply, and substantial pressure fluctuations. To address this problem, this study proposes a surrogate-based fluid supply optimization (SFSO) method in which a continuous supply trajectory is parameterized by a limited number of time–flow control points and reconstructed using a radial basis function model. The control-point parameters are optimized subject to constraints on pump capacity and flow-rate variation, while pressure stability and supply efficiency are considered simultaneously. An AMESim hydraulic system model was validated against measurements obtained from a laboratory hydraulic support platform and was subsequently used to evaluate the proposed method under a predefined multi-support operating sequence. Under 200 independent test scenarios with demand perturbations of up to ±10%, SFSO increased the mean cycle-based volumetric efficiency from 30.16% to 60.10%, representing an increase of 29.94 percentage points. Meanwhile, the mean pressure fluctuation metric J_P decreased from 0.625 MPa^2 to 0.150 MPa^2. Under the model, operating sequence, and demand perturbation range considered in this study, these results indicate that the proposed trajectory-surrogate formulation can improve demand supply matching and reduce the pressure fluctuation index relative to the constant-flow reference. Further work is required to evaluate the method under broader sources of uncertainty and in underground field applications.

Keywords: longwall hydraulic system; fluid-supply optimization; trajectory surrogate; RBF interpolation

Check for updates

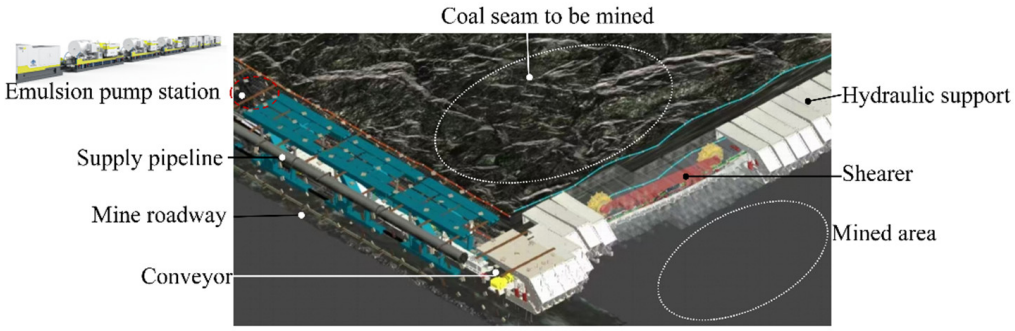
Received: 3 September 2026
Revised: 4 October 2026
Accepted: 16 October 2026
Published: 5 November 2026

Copyright: © 2026 by the authors. Licensee MDPI, Basel, Switzerland. This article is an open access article distributed under the terms and conditions of the Creative Commons Attribution (CC BY) license.

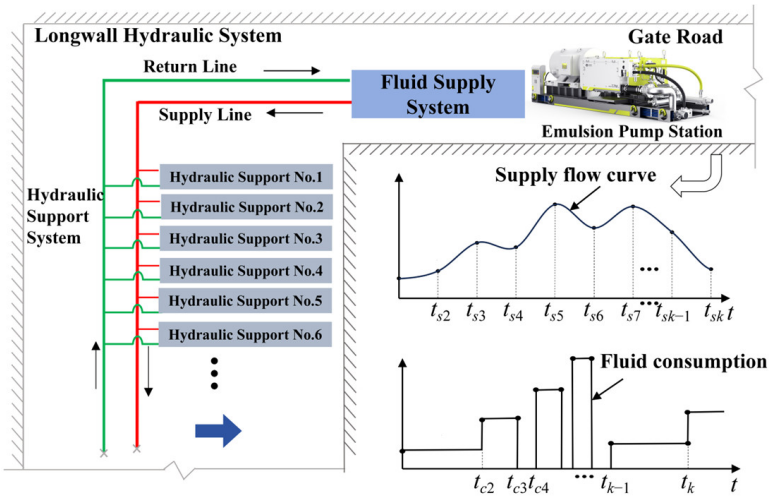
1. Introduction

The longwall mining face is the core unit for high-efficiency coal extraction [1,2]. As illustrated in Figure 1a, its principal equipment comprises a shearer, hydraulic supports, a scraper conveyor, and the associated fluid-supply and control systems. During mining, the shearer moves along the conveyor to excavate coal, while the hydraulic supports sustain the roof and propel the conveyor toward the coal face. The supports are powered by the

longwall hydraulic system [3], which supplies high-pressure, high-flow hydraulic energy for roof support, support advancement, and coordinated equipment operation. Consequently, the performance of the hydraulic system directly affects roof-control effectiveness, equipment coordination, production efficiency, and operational safety [4–6]. Figure 1b shows the configuration and operating principle of the longwall-face hydraulic system. The emulsion pump station, located in the gate road, delivers high-pressure fluid through the main supply line to the hydraulic supports arranged along the coal wall. According to the control commands, the fluid is distributed to the corresponding support actuators and subsequently returns to the pump station through the return line, forming a complete circulation path.



(**a**) Layout of the main equipment



(**b**) Schematic of the hydraulic system

Figure 1. Longwall-face equipment and hydraulic fluid-supply system.

With the increasing coordination and intelligence of longwall equipment, on-demand fluid supply has attracted growing attention [7]. Zeng and Wang [8] developed an adaptive dynamic programming method for optimal pressure tracking, providing an effective solution for single-support column-lifting conditions. Its extension to concurrent and stochastic fluid demand from multiple supports remains to be explored. Cao et al. [9] optimized multi-pump settings and proposed an ADRC-based rapid fluid-replenishment strategy to improve pressure stability under strongly time-varying loads. Their subsequent study further revealed the pressure-impact characteristics of high-pressure, large-flow, long-distance pipelines [10]. These findings provide an important basis for fluid-supply control, although the identified pipeline transients have not yet been explicitly incorporated into supply-trajectory planning and optimization. Tan et al. [11] established a mapping between support actions and pump-station pressure using an Elman neural network, while

Zhang et al. [12] employed PID-based pressure feedback and unloading-valve control to maintain the target pressure range. Peng et al. [13] introduced an online-updating RBF neural network, improving the adaptability of pump-station flow control to changing operating conditions. These studies have advanced pressure stabilization and intelligent pump-station control. However, most focus on pressure regulation under specific support actions or operating conditions, while the coordinated optimization of future fluid demand, pump output, pressure fluctuation, and practical operating constraints remains to be further investigated.

At the actuator level, Hou et al. [14] combined Bang–Bang and predictive control with a multistage throttle valve to coordinate rapid pushing and precise positioning. Wang et al. [15] improved flow-control accuracy through active differential-pressure regulation, while Liao et al. [16] developed a position-following water proportional directional valve for precise and low-impact support control. These precision-control solutions provide valuable approaches for improving actuator performance, although their structural complexity, contamination tolerance, maintainability, and long-term reliability warrant further investigation under underground operating conditions. Overall, existing studies have established a solid foundation in local actuation, pressure regulation, pipeline dynamics, and coordinated operation. Nevertheless, opportunities remain to integrate demand prediction, supply-curve parameterization, multi-objective optimization, fluid-demand disturbances, and engineering constraints into a unified framework for long-distance, nonlinear, and time-varying fluid supply systems.

Hydraulic supports are typically actuated by binary on-off electrohydraulic directional valves that provide only open or closed states, limiting direct flow regulation during operation [17]. As the supports follow the shearer through sequential lowering, advancing, raising, and pushing actions, their flow requirements vary substantially between stages and form a discontinuous demand profile. By contrast, variable-frequency pump stations regulate output continuously through motor speed and therefore produce a comparatively smooth supply profile. Because of motor-pump dynamics, the supply flow cannot immediately reproduce abrupt changes in support demand. Efficient and stable operation therefore requires a planned supply trajectory that coordinates the continuous output of the pump station with the discrete, time-varying demand of the support group.

Fluid demand calculated from support commands and structural parameters represents only the nominal demand. In operation, variable loads, pipeline leakage, and friction affect actuator responses, so identical commands may produce different flow profiles. These deviations are treated here as fluid-demand disturbances. Incorporating them into supply trajectory optimization allows each candidate strategy to be evaluated in terms of pressure stability, supply efficiency, and demand satisfaction over a prescribed disturbance range. Scenario-based optimization provides a practical means of evaluating candidate strategies across a finite set of disturbance realizations [18–20].

Supply-trajectory design can therefore be formulated as a pump-valve cooperative optimization problem that coordinates continuous pump output with discrete actuator demand. Control-point parameterization can reduce a high-dimensional continuous trajectory to a limited set of decision variables [21,22]. Interpolation using splines [23], Bézier curves [24], S-curves [25], or B-splines [26] can then reconstruct a smooth, continuous trajectory from these control points. Accordingly, this study proposes a surrogate-based fluid supply optimization (SFSO) method for longwall hydraulic systems. The method represents the pump-station supply strategy using a limited number of time-flow control points and reconstructs a continuous, differentiable supply trajectory with a cubic radial basis function (RBF) trajectory surrogate. Bounded demand disturbances are introduced over the support-action intervals to generate multiple demand scenarios, and each candi-

date trajectory is evaluated using the corresponding pressure and actuator-flow responses. A genetic algorithm is then employed to optimize the timing and flow rate at each control point, subject to constraints on pump capacity, flow-rate variations, and pressure response, while jointly minimizing pressure fluctuations and supply losses. In this study, the term "surrogate" refers specifically to a low-dimensional continuous representation of the pump-station supply trajectory. The RBF trajectory surrogate replaces direct optimization of a densely discretized control sequence; it does not replace or approximate the AMESim hydraulic system model. Each candidate trajectory is still evaluated directly in AMESim.

The remainder of this study is organized as follows. Section 2 presents the supply trajectory representation and demand-scenario construction. Section 3 formulates the objective function and engineering constraints. Section 4 describes the experimental validation and compares the fluid-supply strategies. Section 5 summarizes the main conclusions.

2. Surrogate-Based Fluid Supply Optimization Method

2.1. Problem Description and Overall Framework

The fluid-supply trajectory of an emulsion pump station must match the dynamic fluid demand of the hydraulic supports. However, the actual fluid demand is inherently uncertain because of variations in hydraulic support operating parameters. Therefore, the optimization of the pump station fluid-supply trajectory is formulated as a constrained continuous optimization problem under uncertain fluid demand. The time positions and flow-rate values of the control points are selected as decision variables. A continuous fluid-supply trajectory is represented by a cubic RBF trajectory surrogate constructed from these control points. Here, the trajectory surrogate replaces a densely discretized control vector, whereas AMESim remains the direct evaluator of the hydraulic response. The control-point parameters are optimized using a genetic algorithm to obtain a trajectory that satisfies the system constraints and accommodates different demand scenarios. The overall optimization procedure consists of the following steps:

(1) Determine the nominal fluid demand curve according to the action sequence and operating parameters of the hydraulic supports.
(2) Divide the hydraulic support operation into action intervals and establish a fluid-demand perturbation model.
(3) Define the fluid-supply control points and their allowable ranges, and construct the continuous RBF trajectory surrogate from these control points.
(4) Check the supply-side constraints, including the pump-station flow rate and its rate of change.
(5) Calculate the system pressure, actuator flow rates, and actual fluid consumption under each demand scenario.
(6) Iteratively update the control-point parameters using a genetic algorithm according to the objective function and constraints.
(7) Once the convergence criterion is satisfied, output the fluid-supply trajectory that meets the system constraints.

Figure 2 illustrates the iterative optimization of the emulsion pump station supply trajectory using the RBF trajectory surrogate. In the nth iteration, the trajectory surrogate is constructed from the current control points and evaluated directly using the AMESim model. The genetic algorithm then updates the time positions and flow-rate values of the control points according to the objective-function value, after which a new trajectory surrogate is constructed in the $(n + 1)$th iteration. This process continues until the termination criterion is reached, and the best feasible solution found in the run is returned.

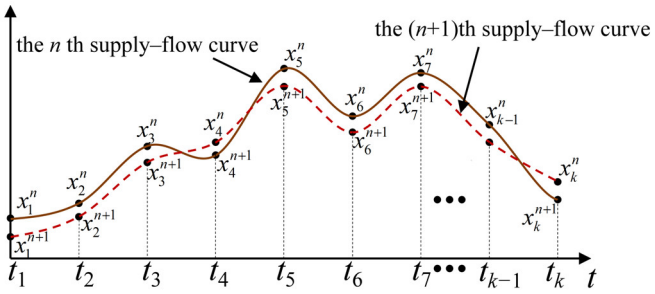


Figure 2. Illustration of surrogate-based fluid supply optimization.

2.2. Surrogate-Based Interpolation and Reconstruction of the Fluid-Supply Trajectory

In the proposed SFSO method, each candidate fluid-supply trajectory is defined by a set of discrete time–flow control points generated by the genetic algorithm. RBF interpolation is employed to reconstruct these control points into a continuous trajectory [27,28]. Unlike conventional data-driven surrogate models, the RBF used here is not intended to learn or predict an unknown input–output relationship. Instead, it provides a deterministic interpolation of the optimization variables, ensuring that the reconstructed trajectory passes through all specified control points while maintaining sufficient smoothness.

Let the fluid-supply trajectory of the emulsion pump station be defined by m control points. The ith control point is expressed as:

$$\boldsymbol{p}_i = (t_i, u_i), \quad i = 1, 2, \ldots, m, \tag{1}$$

where t_i denotes the control-point time and u_i is the corresponding pump-station flow rate. The continuous fluid-supply trajectory is reconstructed as:

$$Q_p(t) = \sum_{i=1}^{m} \lambda_i \phi(|t - t_i|) + a_0 + a_1 t, \tag{2}$$

where $Q_p(t)$ is the pump-station flow rate, λ_i is the RBF weight, $\phi(.)$ is the radial basis function, and $a_0 + a_1 t$ is a first-order polynomial term introduced to ensure the unique solvability of the interpolation system.

The reconstructed trajectory must pass through all control points:

$$Q_p(t_j) = u_j, \quad j = 1, 2, \ldots, m, \tag{3}$$

The RBF weights are also subject to the supplementary conditions:

$$\sum_{i=1}^{m} \lambda_i = 0, \quad \sum_{i=1}^{m} \lambda_i t_i = 0, \tag{4}$$

Accordingly, the interpolation system can be written in matrix form as

$$\begin{bmatrix} \boldsymbol{\Phi} & \boldsymbol{P} \\ \boldsymbol{P}^T & \boldsymbol{0} \end{bmatrix} \begin{bmatrix} \boldsymbol{\lambda} \\ \boldsymbol{a} \end{bmatrix} = \begin{bmatrix} \boldsymbol{u} \\ \boldsymbol{0} \end{bmatrix}, \tag{5}$$

where

$$\Phi_{ij} = \phi(|t_i - t_j|), \quad \mathrm{P} = \begin{bmatrix} 1 & t_i \\ 1 & t_2 \\ \vdots & \vdots \\ 1 & t_m \end{bmatrix}, \tag{6}$$

and

$$\boldsymbol{\lambda} = [\lambda_1, \lambda_2, \ldots, \lambda_m]^T, \ \boldsymbol{a} = [a_0, a_1]^T, \ \boldsymbol{u} = [u_1, u_2, \ldots, u_m]^T, \tag{7}$$

Solving Equation (5) yields the RBF weights and polynomial coefficients, from which the continuous fluid-supply trajectory over the entire operating period can be obtained. Common RBF kernels include Gaussian, multiquadric, inverse multiquadric, and cubic functions. Although the first three kernels can produce smooth curves, their interpolation results and matrix conditioning are sensitive to the choice of shape parameters. An inappropriate shape parameter may excessively smooth rapid demand variations or result in an ill-conditioned interpolation matrix. Therefore, the cubic RBF is adopted in this study:

$$\phi(r) = r^3, \tag{8}$$

The cubic RBF requires no additional shape parameter, strictly interpolates all control points, and produces a smooth trajectory with a continuous first derivative. These properties allow it to serve as a deterministic trajectory surrogate. Because only a small number of control points are involved, each candidate trajectory surrogate can be constructed by solving a small linear system, resulting in a relatively low computational cost compared with the repeated AMESim evaluations required by the genetic algorithm.

The cubic RBF is selected according to the specific requirements of the present trajectory-representation task: exact interpolation of deterministic control points, smoothness, and repeated low-cost construction during optimization. This task differs from learning an unknown input–output relationship from training data, for which Kriging, artificial neural networks, or support vector regression may be appropriate. The present study therefore does not claim that the cubic RBF is generally superior to these methods. Future work may compare alternative trajectory surrogate constructions in terms of reconstruction accuracy, smoothness, computational cost, and robustness.

To maintain the correct temporal order of the control points and prevent excessive clustering, the following constraints are imposed:

$$t_1 = 0, t_m = T, t_{i+1} - t_i \geq \Delta t_{\min}, i = 1, 2, \ldots, m-1, \tag{9}$$

where T is the complete operating cycle of the hydraulic supports and $\Delta t_{\min}$ is the minimum allowable interval between adjacent control points.

The optimization vector consists of the internal control-point times and the flow rates of all control points:

$$\boldsymbol{X} = [t_2, t_3, \ldots, t_{m-1}, u_1, u_2, \ldots, u_m]^T, \tag{10}$$

Because the initial and terminal times are fixed at 0 and T, respectively, the dimension of the optimization vector is

$$d(\boldsymbol{X}) = 2m - 2, \tag{11}$$

2.3. Construction of Fluid-Demand Perturbation Scenarios

Let $Q_d^0(t)$ denote the nominal fluid-demand curve calculated from the operating sequence of the hydraulic supports, the structural parameters of the actuators, and the nominal operating speeds. Owing to variations in operating speed, load, and valve response, the actual fluid demand may fluctuate around its nominal value. To characterize demand uncertainty associated with different hydraulic-support operations, the complete operating cycle is divided into K action intervals:

$$[0, T] = \bigcup_{k=1}^{K} I_k, I_k = [\tau_{k-1}, \tau_k], \ 0 = \tau_0 < \tau_1 < \cdots < \tau_K = T, \tag{12}$$

where each interval may correspond to support lowering, support advancing, support raising, or conveyor pushing. In the s th random scenario, the fluid demand within the kth action interval is expressed as

$$Q_d^{(s)} = Q_d^0(t)\left[1 + \rho\xi_k^{(s)}\right], \quad t \in I_k, \tag{13}$$

where ρ is the maximum relative perturbation amplitude of the fluid-demand flow rate, and $\xi_k^{(s)}$ is the dimensionless perturbation variable for the kth action interval in the sth scenario. Here, $s = 1, 2, \ldots, S$ is the scenario index, and S is the number of perturbation scenarios used during optimization. The perturbation variable is assumed to follow a uniform distribution over $[-1, 1]$:

$$\xi_k^{(s)} \sim U[-1, 1], \tag{14}$$

Accordingly, the sth scenario can be represented by a complete perturbation vector:

$$\boldsymbol{\xi}^{(s)} = \left[\xi_1^{(s)}, \xi_2^{(s)}, \ldots, \xi_K^{(s)}\right], \tag{15}$$

Each perturbation vector represents a possible actual fluid-demand state over the complete operating cycle and generates a corresponding perturbed demand curve. When the perturbation coefficients in all action intervals are zero, the nominal fluid-demand scenario is obtained:

$$\boldsymbol{\xi}^{(0)} = \mathbf{0}, \quad Q_d^{(0)}(t) = Q_d^0(t), \tag{16}$$

A constant perturbation coefficient is applied within each action interval to avoid introducing physically unjustified high-frequency fluctuations between adjacent sampling points. The coefficients are sampled separately for different intervals to reflect variations in load, valve response, and leakage among different hydraulic-support operations.

To ensure that the fitness values of different candidate fluid-supply trajectories are comparable, a fixed set of perturbation scenarios is used throughout the genetic-algorithm optimization. Thus, all candidate solutions are evaluated using the same random samples. After optimization, an independent set of test scenarios that was not used during optimization is generated to evaluate the adaptability of the resulting fluid-supply trajectory to previously unseen demand perturbations and to prevent overfitting to the optimization scenarios.

2.4. Solution Procedure for Fluid-Supply Trajectory Planning

For each candidate solution $\boldsymbol{X}$ generated by the genetic algorithm (GA), a cubic RBF trajectory surrogate is constructed to represent the continuous fluid-supply trajectory $Q_p(t)$. The trajectory is evaluated on a refined time grid to verify the pump-flow and flow-rate variation constraints. Each feasible trajectory is then evaluated using the computational model under S fixed fluid-demand scenarios.

$$\boldsymbol{X} \rightarrow Q_p(t) \rightarrow \begin{cases} Q_d^{(1)}(t) \rightarrow J^{(1)} \\ Q_d^{(2)}(t) \rightarrow J^{(2)} \\ \quad\vdots \\ Q_d^{(S)}(t) \rightarrow J^{(S)} \end{cases}, \tag{17}$$

After all individuals in the current population have been evaluated, the GA updates the control-point parameters through selection, crossover, and mutation. A candidate that violates the pump-flow, flow-rate-variation, or demand-satisfaction constraints is assigned an infeasible fitness and is excluded from selection or replaced when the next population is generated. This replacement is part of the GA population update and

does not represent adaptive resampling of a system-response-surrogate training set. The optimization terminates when the maximum number of generations is reached. The best feasible individual is then returned as the supply trajectory. The complete SFSO procedure is summarized in Table 1 and Figure 3.

Table 1. Pseudocode of the SFSO method.

The surrogate-based fluid supply optimization procedure
1: Determine the feasible domain of the control points, the fixed demand-disturbance scenarios, and the engineering constraints;
2: Initialize the candidate control-point solutions;
3: **while** the convergence criterion is not satisfied and the maximum number of generations has not been reached **do**
4: Construct the RBF trajectory surrogate from the candidate control points;
5: Discretize the trajectory and evaluate the supply-side constraints;
6: Evaluate feasible trajectories under the fixed demand-disturbance scenarios;
7: Calculate the pressure-fluctuation, supply-loss, and unmet-demand indices and determine the robust fitness;
8: Assign infeasible fitness to candidates that violate the engineering constraints;
9: Update the candidate population through selection, crossover, and mutation;
10: **end while**
11: **Output the optimalfluidsupply trajectory**

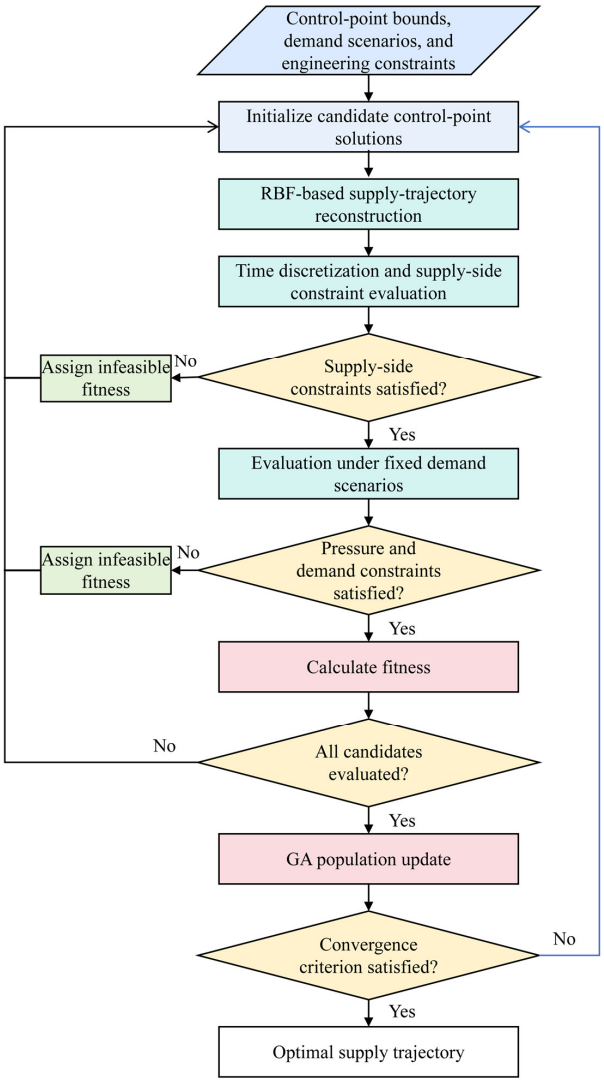


Figure 3. Overall procedure of the SFSO method.

3. Fluid Supply Optimization Problem Formulation

3.1. Objective Function

Excessive pressure fluctuations can reduce the operating stability of the hydraulic supports, accelerate fatigue and wear in the valves and pipelines, and potentially cause frequent activation of the relief valve. To evaluate pressure stability under the s th fluid-demand scenario, the variance of the pressure changes between adjacent sampling instants is adopted as the pressure-fluctuation index:

$$J_P^{(s)} = \frac{1}{N-1}\sum_{i=1}^{N-1}\left[(P_{i+1}^{(s)} - P_i^{(s)}) - \overline{\Delta P}^{(s)}\right]^2, \tag{18}$$

where $P_i^{(s)}$ is the system pressure at the ith sampling instant under scenario s; N is the total number of sampling points; and $\overline{\Delta P}^{(s)}$ is the mean pressure change between adjacent sampling points. A smaller pressure-fluctuation index indicates a more stable pressure response.

A portion of the flow supplied by the emulsion pump station enters the actuators to perform hydraulic-support operations, while the excess flow returns to the reservoir through overflow or unloading, resulting in energy losses and an increase in fluid temperature. The fluid-supply efficiency under scenario s is defined as

$$\eta^{(s)} = \frac{V_{\text{act}}^{(s)}}{V_{\text{sup}}^{(s)}}, \tag{19}$$

where

$$V_{\text{act}}^{(s)} = \int_0^T Q_{\text{act}}^{(s)}(t)\mathrm{d}t,\ V_{\text{sup}} = \int_0^T Q_p(t)\mathrm{d}t, \tag{20}$$

V_{sup} is the total volume supplied by the pump station over the complete operating cycle, and $V_{\text{act}}^{(s)}$ is the fluid volume delivered to the hydraulic-support actuators to perform effective operations under scenario s.

The corresponding fluid-supply loss index is

$$J_l^{(s)} = 1 - \eta^{(s)}, \tag{21}$$

A smaller value indicates higher fluid utilization and lower unnecessary overflow losses. Because the pressure-fluctuation and fluid-supply loss indices differ in both dimensions and magnitudes, they are normalized as follows:

$$J_{i,\text{norm}}^{(s)} = \frac{J_i^{(s)} - J_i^{\min}}{J_i^{\max} - J_i^{\min}}, i = P, l, \tag{22}$$

The composite performance index under scenario s is then defined as

$$J^{(s)} = \sum_i \omega_i J_{i,\text{norm}}^{(s)}, i = P, l, \tag{23}$$

where w_i denotes the weight of each sub-objective. After min–max normalization, the objectives are dimensionless and comparable. Equal weights are adopted because neither pressure stability nor supply efficiency is prioritized in this study. A larger pressure weight favors a smoother pressure response, whereas a larger efficiency weight promotes closer

demand matching and lower overflow losses. The weights can be adjusted according to field operating requirements.

$$J_{\mathrm{rob}}(\boldsymbol{X}) = \frac{1}{S}\sum_{s=1}^{S} J^{(s)}(\boldsymbol{X}), \tag{24}$$

The resulting optimization problem is formulated as follows:

$$\min_{\boldsymbol{X}} J_{\mathrm{rob}}(\boldsymbol{X}), \tag{25}$$

3.2. Constraint Formulation

The fluid supply is centrally regulated and delivered by the emulsion pump station. The station adjusts the drive motor speed via a variable-frequency drive to achieve continuous flow control. Due to the inherent electromechanical characteristics of the motor-pump unit, the flow rate must satisfy smoothness and magnitude constraints. The main constraints are summarized as follows:

(1) Lower bound on pump flow rate

Frequent start-stop cycles and very low motor speeds can accelerate wear and cause overheating, compromising pump and motor reliability. To ensure long-term stable operation, a minimum pump flow Q_p must be maintained, given its near one-to-one relationship with motor speed:

$$Q_p = k_{\mathrm{p}} \cdot n_{\mathrm{motor}}, \tag{26}$$

where k_{p} is the pump flow coefficient. To avoid poor lubrication and frequent start-stops, the motor speed n_{motor} must remain above a minimum threshold n_{min}, leading to the following flow rate constraint:

$$Q_p(t) \geq Q_{\mathrm{min}} = k_{\mathrm{p}} \cdot n_{\mathrm{min}}, \tag{27}$$

(2) Pump capacity constraint

The instantaneous flow of each pump must lie within its rated safe range:

$$Q_p(t) \leq Q_{\mathrm{max}}, \tag{28}$$

where Q_{max} represents the maximum safe operating flow rate of the pump.

(3) Flow variation constraint

Considering the dynamic response limitations of pumps and valves, abrupt changes in flow can induce hydraulic shocks or valve overshoot. Therefore, the flow change per sampling period is constrained:

$$|\, Q_p(t_{i+1}) - Q_p(t_i) \,| \leq \Delta Q_{\mathrm{max}}, \tag{29}$$

where ΔQ_{max} is determined by the pump-valve response characteristics and the inertia of the hydraulic network, ensuring smooth operation of support actions.

(4) Fluid-demand satisfaction constraint

Fluid-supply efficiency primarily reflects the degree of excess supply, but it cannot independently determine whether the demand of the hydraulic supports is adequately satisfied. If supply efficiency alone is maximized, the optimization algorithm may achieve an apparently high utilization rate by reducing the supply flow, potentially slowing the hydraulic-

support operations or preventing their completion. Therefore, the unmet-demand ratio under scenario s is defined as

$$J_u^{(s)} = \frac{\int_0^T \max\left[Q_d^{(s)}(t) - Q_{\text{act}}^{(s)}(t), 0\right] \mathrm{d}t}{\int_0^T Q_d^{(s)}(t) \mathrm{d}t}, \tag{30}$$

A value of $J_u^{(s)} = 0$ indicates that the fluid demand is fully satisfied throughout the operating cycle, whereas a larger value indicates a more severe supply shortage. The following constraint is imposed:

$$\max_{s=1,\ldots,S} J_u^{(s)} \leq \varepsilon_u, \tag{31}$$

where ε_u is the maximum allowable unmet-demand ratio.

The constraints of the robust fluid-supply optimization problem can be written compactly as:

$$g = \begin{bmatrix} g_1 \\ g_2 \\ g_3 \\ g_4 \end{bmatrix} = \begin{bmatrix} Q_{\min} - Q_p(t) \\ Q_p(t) - Q_{\max} \\ \left|Q_p(t_{i+1}) - Q_p(t_i)\right| - \Delta Q_{\max} \\ \max\limits_{s=1,\ldots,S} J_u^{(s)} - \varepsilon_u \end{bmatrix} \leq \mathbf{0}, \tag{32}$$

4. Experimental Study

4.1. Experimental Platform and Simulation Model Validation

To validate the AMESim model used for the subsequent comparison of fluid-supply strategies, an experimental hydraulic-support platform was established, and sensors were installed on the key actuating components of the hydraulic support to continuously measure pressure and flow rate variations under different operating conditions, as illustrated in Figure 4. The technical parameters of the hydraulic support are listed in Table 2. The supply and return flow rates were measured using HYDROTECHNIK turbine flowmeters (HTF/33JC-78-35.V012G), with a measuring range of 15–300 L/min and an accuracy of ±0.5% of the measured value. The pressure at the supply and return lines, the front and rear chambers of the pushing cylinder, and the upper and lower chambers of the support columns was measured using HYDROTECHNIK HySense PR110 pressure sensors (3403-15-C3.37). The pressure sensors have a measuring range of 0–400 bar, an accuracy of less than ±0.5% of full scale, and a response time of less than 1 ms. The flowmeters provide frequency signals, whereas the pressure sensors provide two-wire 4–20 mA signals. All measuring channels were calibrated before testing and sampled synchronously by the data-acquisition system.

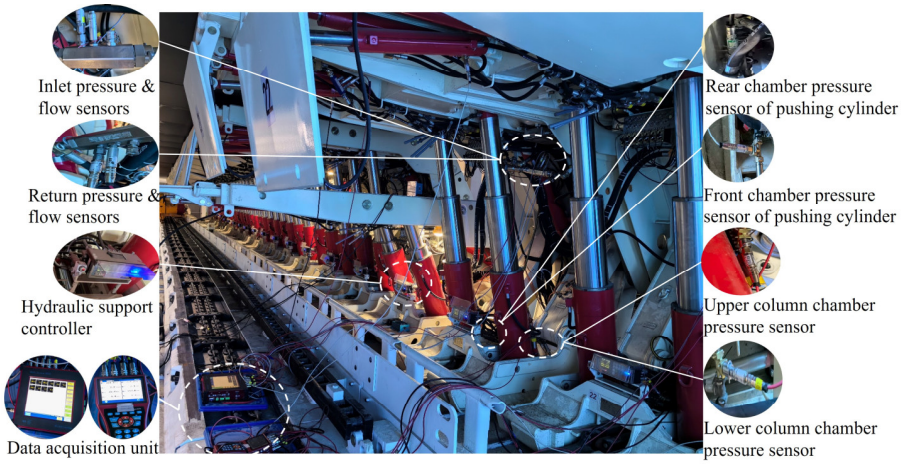


Figure 4. Sensor layout on the experimental platform.

Table 2. Technical parameters of the experimental platform

Parameters	Value
Hydraulic support height	1250–2600 mm
Hydraulic support width	1400–1500 mm
Mass	10,134.3 kg
Working resistance	3200 kN (P = 38.5 MPa)
Initial support force	2616 kN (P = 31.5 MPa)
Maximum supply pressure of pump station	35 MPa
Support columns cylinder diameter	420/395 mm
Propelling cylinder diameter	200/140 mm
Electro-hydraulic control valve	500 L/min
Hydraulic control check valve	400 L/min
Frame pulling hydraulic control check valve	100 L/min
Inlet pipeline specification	DN25
Return pipeline specification	DN32

In the process of optimizing fluid supply for longwall hydraulic systems, it is essential to systematically and quantitatively evaluate the performance of different supply trajectories to guide the optimization iterations. Accordingly, a comprehensive AMESim model was developed based on the system's physical mechanisms and control logic (Figure 5). The model comprises an adjustable-flow supply unit, support lifting and shifting modules, and auxiliary hydraulic components. The variable-speed motor and fixed-displacement pump were simplified as a constrained controllable flow source, with rated-flow and flow-rate variation limits imposed to ensure feasible supply commands. This representation is appropriate for system-level comparisons because all strategies are evaluated using identical plant models and operating conditions. However, it excludes rotational inertia, motor torque–speed characteristics, variable-frequency-drive dynamics, and operating-point-dependent pump efficiency, and may therefore overestimate transient tracking performance. Before field implementation, a coupled motor–drive–pump model calibrated against measured speed and flow responses will be required. Because this study focuses on the methodological evaluation of supply strategies, the supply-pipeline parameters were fixed at values representative of the investigated hydraulic system. This controlled configuration isolates the interaction between support-side demand and pump-station supply from variations in pipeline dynamics. The results are therefore specific to this configuration. Although pipeline length influences hydraulic resistance, fluid inertia, and pressure-wave propagation [29], its systematic sensitivity analysis lies beyond the scope of this methodological study.

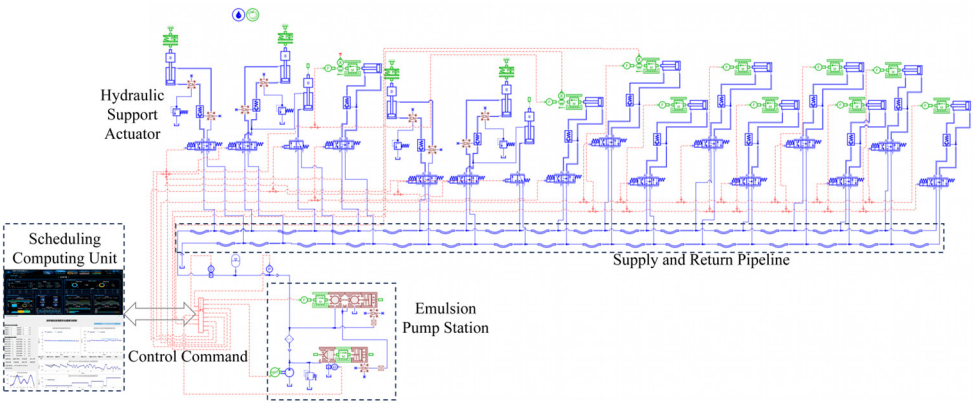
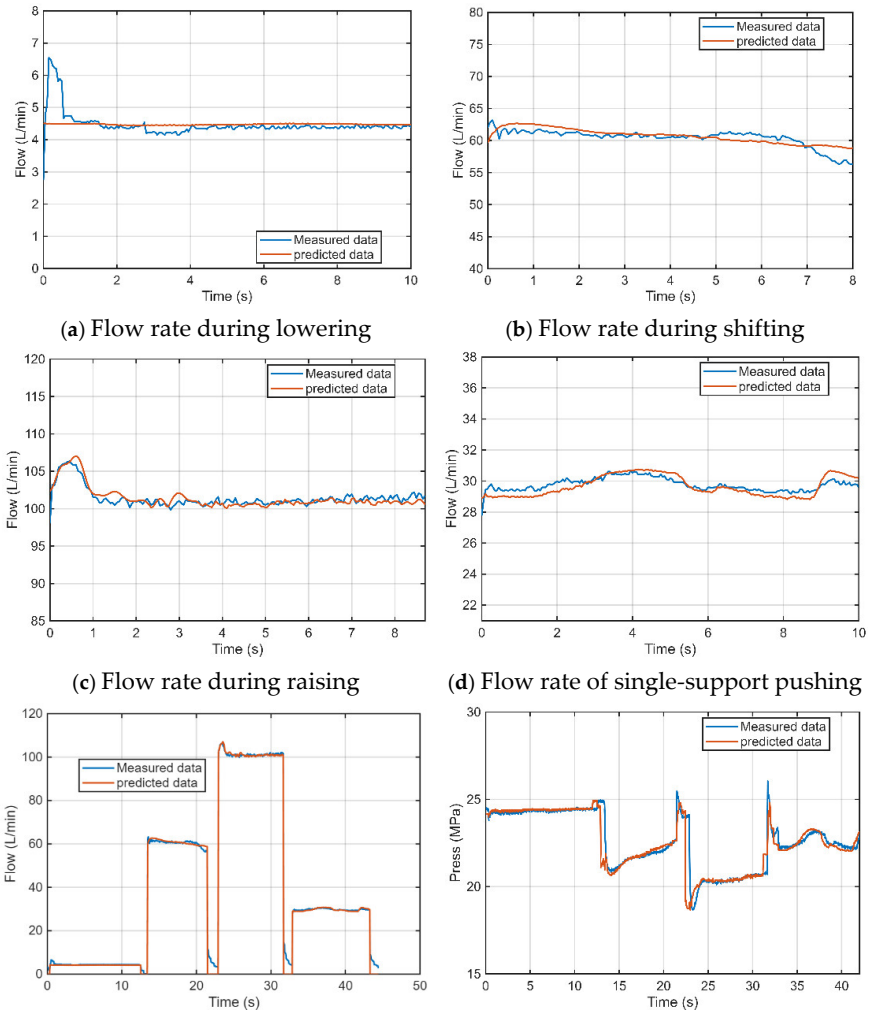


Figure 5. Support hydraulic system simulation model.

During simulation, the scheduling computing unit sends specific motion commands to the hydraulic model. The model calculates the dynamic responses of the hydraulic supports and actuators, and then returns the results to the scheduling unit for analysis. Pressures and flow rates during key hydraulic support operations were calculated using the simulation model and compared with experimental measurements to validate its accuracy, as shown in Figure 6. To quantitatively evaluate the accuracy of the simulation model, the measured and simulated signals shown in Figure 6 were aligned in time, and their errors were calculated over the complete test interval, including both steady-state and transient periods. Because flow rate and pressure have different physical units and numerical scales, they were evaluated separately using the mean absolute error (MAE) and root-mean-square error (RMSE). For the flow-rate responses, MAE = 0.979 L/min and RMSE = 2.06 L/min. For the pressure responses, MAE = 0.295 MPa and RMSE = 0.791 MPa. The higher RMSE values relative to the corresponding MAE values indicate that the principal discrepancies are concentrated around rapid transient changes. Nevertheless, the model accurately reproduces the overall trends and principal dynamic characteristics of the measured flow and pressure responses. These results indicate that the model reproduces the overall flow and pressure trends under the tested conditions. However, the remaining model error should be considered when interpreting differences among the fluid-supply strategies.



(**a**) Flow rate during lowering

(**b**) Flow rate during shifting

(**c**) Flow rate during raising

(**d**) Flow rate of single-support pushing

(**e**) Flow rate for continuous operations

(**f**) Pressure for continuous operations

Figure 6. Comparison of measured and simulated flow and pressure responses.

4.2. Hydraulic Support Operating Sequence and Fluid-Demand Perturbation Scenario Settings

To ensure consistent comparisons among different fluid-supply strategies, the same hydraulic support operating sequence is used in all tests. The first hydraulic support performs leg lowering for 10 s, followed by a 2 s pause; support advancing for 7 s, followed by a 2 s pause; and leg raising for 7 s, followed by another 2 s pause. The second hydraulic support then performs the same sequence of operations. After these operations are completed, all five hydraulic supports simultaneously push the conveyor for 5 s, followed by a 5 s pause. The complete operating sequence is illustrated in Figure 7.

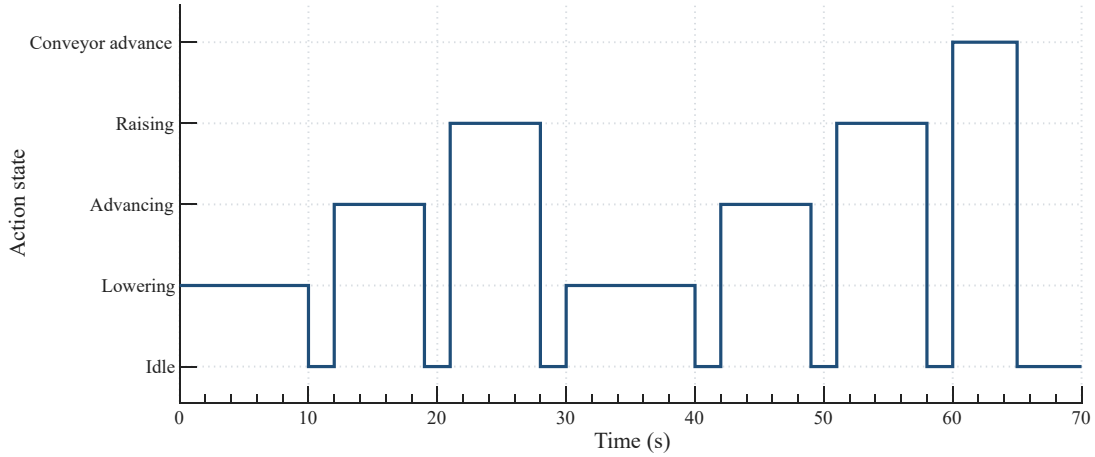


Figure 7. Timing diagram of the hydraulic support operations.

Based on the operating sequence and hydraulic support parameters, the instantaneous flow demand of each actuator under rated operating conditions is calculated. The flow rates of simultaneously operating actuators are then superimposed to obtain the nominal fluid-demand curve over the complete 70 s operating cycle. According to the switching times of the hydraulic support operations, the cycle is divided into seven action intervals.

Because of the randomness of hydraulic support operations, the predicted flow demand may contain errors. Random perturbations are therefore introduced during optimization. A uniform perturbation coefficient is applied within each action interval to avoid physically unjustified high-frequency fluctuations between adjacent sampling points. The coefficients are sampled separately for different intervals to represent their different sensitivities to variations in load, valve response, and leakage. To evaluate the proposed robust fluid-supply optimization method under moderate demand uncertainty, the maximum relative demand perturbation is set to 10%.

During optimization, 15 random demand scenarios are generated. One nominal scenario and two boundary scenarios representing uniformly high and low demands are also included. A fixed scenario set is used throughout the genetic-algorithm optimization to ensure comparable fitness evaluations among candidate trajectories. After optimization, 200 independent test scenarios are generated using a different random seed. The optimized fluid-supply control points remain unchanged during testing to evaluate the adaptability of the resulting trajectory to previously unseen demand perturbations.

4.3. Comparative Method and Optimization Parameters

To validate the effectiveness of the surrogate-based fluid-supply trajectory optimization method, a constant-flow strategy with pressure-triggered unloading (CFS) is used as the benchmark. Under this strategy, the pump station maintains its rated flow output throughout the complete operating cycle and does not adjust the supply flow according to

the demand of the hydraulic supports. The unloading valve is switched solely according to the system pressure. This strategy is currently widely used in practical applications.

The two strategies employ exactly the same hydraulic system model, hydraulic support operating sequence, pump-station capacity constraints, and flow-rate variation constraint. The SFSO fluid-supply trajectory is parameterized using 15 initial control points. The times of the first and last control points are fixed at 0 and 70 s, respectively, whereas the temporal positions of the remaining control points and the flow-rate values of all control points are treated as optimization variables. The genetic algorithm uses a population size of 50 and a maximum of 100 generations. The weights assigned to pressure fluctuation and fluid-supply loss are both set to 0.5. The maximum allowable unmet-flow ratio is set to 5%. The parameter settings for fluid-supply trajectory optimization are summarized in Table 3.

Table 3. Parameters for fluid-supply trajectory optimization.

Parameter	Symbol	Value
Complete operating cycle	T	70 s
Number of fluid-supply control points	m	15
Genetic algorithm population size	N_{pop}	50
Maximum number of generations	N_{gen}	100
Weight of pressure fluctuation	w_{p}	0.5
Weight of fluid-supply loss	w_{l}	0.5
Number of stochastic scenarios used for optimization	S	18
Number of independent test scenarios	S_{test}	200
Minimum time interval between control points	$\Delta t_{\min}$	1.5 s
Minimum pump-station supply flow rate	$Q_{\min}$	50 L/min
Maximum pump-station supply flow rate	$Q_{\max}$	200 L/min
Maximum allowable unmet-flow ratio	ε_u	5%

Figure 8 shows the variation in the objective function value with the number of iterations, while Figure 9 illustrates the evolution of the SFSO fluid-supply trajectory at different stages of the optimization process. During the initial iterations, the fluid-supply trajectory deviates considerably from the fluid-demand curve. At this stage, the genetic algorithm performs broad exploration of the solution space and rapidly updates the time and flow-rate values of the control points, leading to a substantial decrease in the objective function value. As the optimization proceeds, the supply flow gradually increases during the main hydraulic-support operations and decreases during the pressure-holding and inactive intervals, thereby improving the agreement between the fluid-supply and fluid-demand trajectories. Meanwhile, the control-point positions and their corresponding flow rates progressively stabilize, and the reduction in the objective function value becomes more gradual, indicating convergence of the optimization process. The optimized control points are located at 0, 6.19, 8.96, 12.83, 20.73, 22.92, 28.99, 33.52, 37.78, 46.08, 48.61, 55.38, 60.32, 63.09, and 70 s, with corresponding flow rates of 67, 68, 74, 98, 87, 110, 119, 153, 83, 67, 77, 77, 111, 166, and 53 L/min, respectively. The final fluid-supply trajectory satisfies the pump-flow and flow-rate variation constraints while closely following the overall trend of the hydraulic-support fluid demand.

To compare the performance of the two fluid-supply strategies, Figure 10 presents the system pressure and supply and demand flow rates obtained using CFS and SFSO. Because CFS maintains a constant supply flow, it cannot dynamically adjust the pump-station output according to the demand at different stages of hydraulic-support operation. During pressure-holding or inactive periods, the supplied flow substantially exceeds the actual demand, resulting in temporary oversupply. The excess flow is discharged through overflow or unloading, causing hydraulic energy losses and reducing the overall supply

efficiency. Moreover, the mismatch between supply and demand tends to increase system-pressure fluctuations, which is detrimental to stable hydraulic-system operation.

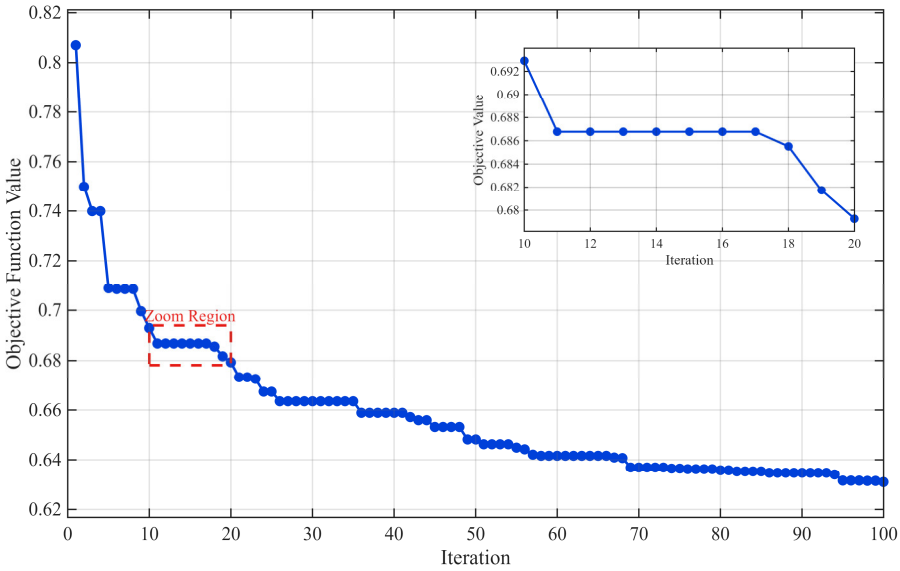


Figure 8. Objective function convergence process.

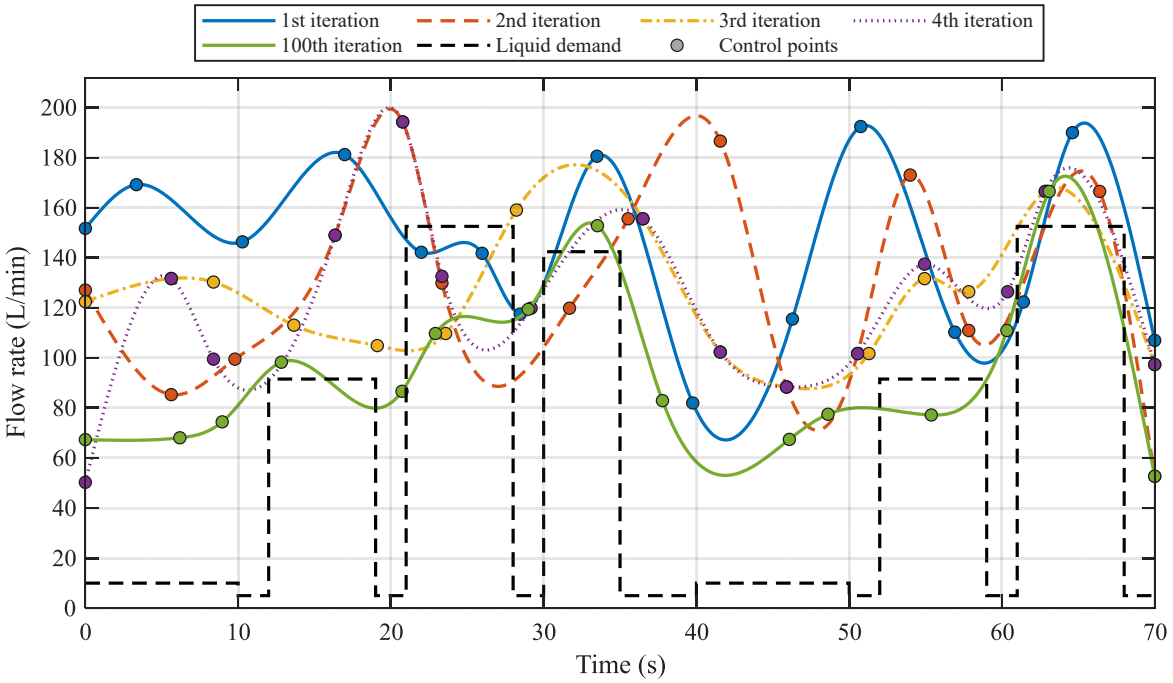
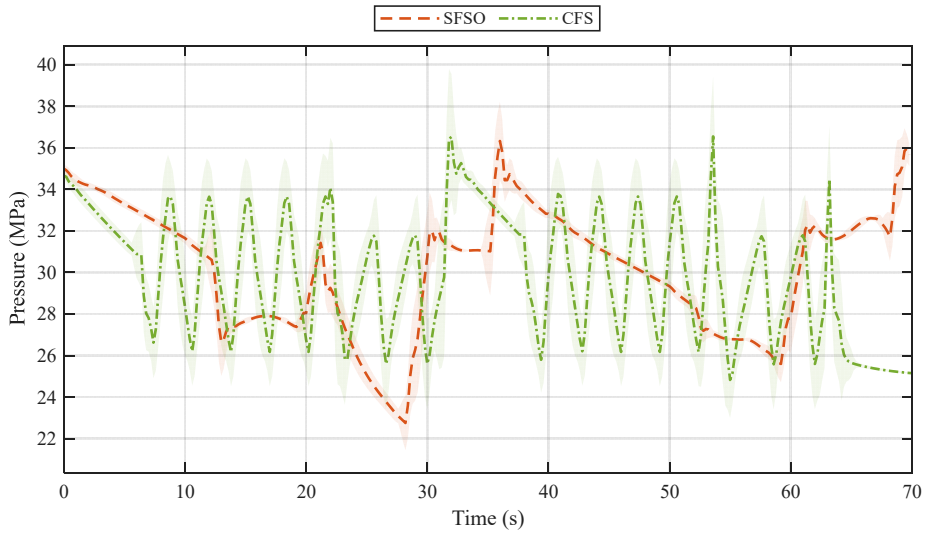


Figure 9. Evolution of the fluid-supply trajectory during optimization.

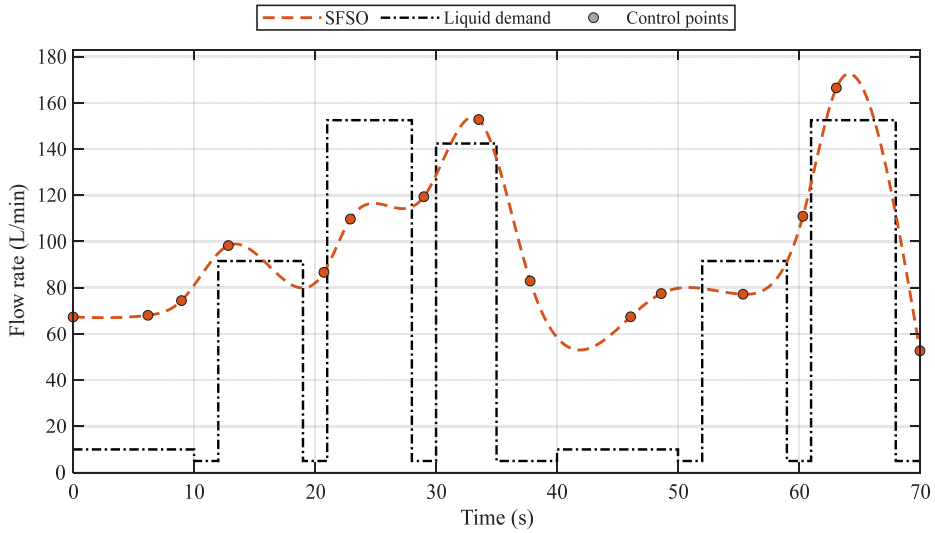
By contrast, SFSO optimizes the time positions and flow-rate values of the supply control points, allowing the pump-station output to vary with the hydraulic-support demand. The supply flow is increased during high-demand operations, such as support advancing, raising, and conveyor pushing, and reduced during lowering and inactive periods. This improves the matching between supply and demand.

After RBF reconstruction, the fluid-supply trajectory remains continuous and smooth, avoiding abrupt flow changes between adjacent control points. The reconstructed trajectory satisfies the imposed flow-rate-variation constraint; its tracking performance with detailed motor–drive–pump dynamics remains to be validated. These results demonstrate that

adjusting the pump-station output according to the stage-dependent demand of the hydraulic supports can reduce unnecessary overflow and unloading losses, improve supply efficiency, and enhance system-pressure stability.



(**a**) Pressure fluctuation



(**b**) Optimized supply and demand curves

Figure 10. Comparison between CFS and SFSO.

To quantify the overall performance of the two fluid-supply strategies more accurately, 200 independent test scenarios that were not used during optimization were randomly generated with the maximum relative perturbation amplitude set to 10%. To ensure a fair comparison, identical fluid-demand inputs were applied to both SFSO and CFS. The pressure-fluctuation index and cycle-based volumetric efficiency were calculated for each strategy under every demand-perturbation scenario. The statistical results are presented in Table 4.

Table 4. Performance of different fluid supply strategies under demand perturbations.

Fluid Supply Strategy	Mean J_P (MPa^2)	*95th Percentile of* J_P (MPa^2)	Mean η (%)	*95th Percentile of* η (%)
CFS	0.625	0.699	30.16%	30.43%
SFSO	0.150	0.155	60.10%	60.19%

Compared with CFS, SFSO reduced the mean pressure-fluctuation index by 0.475 MPa^2 and its 95th-percentile value by 0.544 MPa^2. These results indicate that SFSO reduces pressure fluctuations not only under typical perturbation conditions but also in scenarios with relatively pronounced fluctuations. In terms of fluid-supply efficiency, SFSO increased the mean cycle-based volumetric efficiency by 29.94 percentage points and its 95th-percentile value by 29.76 percentage points. This demonstrates that SFSO improves the matching between the pump-station supply and the actual demand of the hydraulic supports, thereby reducing the energy losses caused by overflow and unloading. Within the tested ±10% demand perturbation range, SFSO produced a lower pressure-fluctuation index and a higher cycle-based volumetric efficiency than CFS.

5. Conclusions

This paper proposes a surrogate-based fluid supply optimization (SFSO) method for the time-varying fluid demand of hydraulic supports. The method uses a limited number of time–flow control points and a cubic RBF trajectory surrogate to represent the complete continuous supply command in a low-dimensional form. The trajectory surrogate replaces a densely discretized control vector, while the hydraulic response of every candidate trajectory is evaluated directly using the AMESim model. Validation against experimental data demonstrates that the AMESim model can reproduce the principal dynamic characteristics of the system's flow and pressure responses. The flow MAE and RMSE are 0.979 L/min and 2.06 L/min, respectively, while the pressure MAE and RMSE are 0.295 MPa and 0.791 MPa, respectively. Across 200 independent test scenarios with demand perturbations of no more than ±10%, SFSO reduces the mean pressure fluctuation metric from 0.625 MPa^2 to 0.150 MPa^2 and its 95th-percentile value from 0.699 MPa^2 to 0.155 MPa^2 compared with the conventional constant-rated-flow supply strategy. It also increases the mean cycle-based volumetric efficiency from 30.16% to 60.10%, an improvement of 29.94 percentage points. These results indicate that, under the model and operating conditions considered in this study, adjusting pump-station output according to the operating stages of the hydraulic supports can improve supply–demand matching, reduce ineffective fluid supply during low-demand periods, and mitigate system pressure fluctuations.

It should be noted that the constant-flow strategy with pressure-triggered unloading serves only as a reference for conventional operation rather than as a baseline representing an advanced control method. Therefore, the above results do not establish the general superiority of SFSO. The current validation is limited to a laboratory platform and AMESim simulations involving a limited number of hydraulic supports. Moreover, the adopted perturbation model describes only variations in demand magnitude within individual operating intervals and does not account for shifts in action timing, sensor noise, communication delays, parameter drift, or pressure-wave propagation in long-distance pipelines. In addition, the current optimization is performed offline for a predefined action sequence; its real-time performance and applicability at the scale of a complete longwall face remain to be verified. Future research will use field data to identify the characteristics of actual demand perturbations, further account for action-timing errors, variations in model parameters, and measurement uncertainty, and investigate fluid supply control methods integrating online state estimation with receding-horizon optimization. Multi-support experiments, long-pipeline tests, hardware-in-the-loop validation, and underground field trials will also be conducted to systematically evaluate the method's real-time performance, robustness, safety, and scalability.

Author Contributions: Conceptualization, T.F.; methodology, T.F. and R.Z.; software, T.F.; validation, T.F. and R.Z.; formal analysis, T.F.; investigation, T.F. and R.Z.; resources, R.Z.; data curation, T.F.; writing—original draft preparation, T.F.; writing—review and editing, T.F. and R.Z.; visualization, T.F.; supervision, R.Z.; project administration, R.Z.; funding acquisition, T.F. All authors have read and agreed to the published version of the manuscript.

Funding: This research was supported by the China Postdoctoral Science Foundation-CCTEG Joint Support Program (2025T029ZGMK), the Science and Technology Innovation Fund of China Coal Technology and Engineering Group (2026-TD-QN-008), and the TMIC Project of China (2025-TM-013-J1 and 2025-TM-021-J1).

Data Availability Statement: The data sets and codes used in this paper to support the finding of this study are available from the corresponding author upon request.

Conflicts of Interest: Authors Tao Fu and Rulin Zhou were employed by the Beijing Tianma Intelligent Control Technology Co., Ltd. All authors declare that the research was conducted in the absence of any commercial or financial relationships that could be construed as a potential conflict of interest.

Nomenclature

SFSO	surrogate-based fluid supply optimization
CFS	constant-flow strategy with pressure-triggered unloading
RBF	radial basis function
SVR	support vector regression
ANN	artificial neural network
$Q_p(t)$	pump-station flow rate
λ_i	RBF interpolation weight
$\phi(.)$	radial basis function
$\Delta t_{\min}$	minimum allowable interval between adjacent control points
$\boldsymbol{X}$	optimization decision vector
s	scenario index
K	number of hydraulic-support action intervals
$Q_d^0(t)$	nominal fluid-demand flow rate
$Q_d^{(s)}(t)$	fluid-demand flow rate under scenario s
$\xi_k^{(s)}$	perturbation variable for action interval k under scenario s
ρ	maximum relative demand-perturbation amplitude
$J_P^{(s)}$	pressure-fluctuation index under scenario s
$P_i^{(s)}$	system pressure at sampling instant i under scenario s
N	total number of sampling points
$\eta^{(s)}$	cycle-based volumetric efficiency under scenario s
$\overline{\Delta P}^{(s)}$	mean pressure change between adjacent sampling points
V_{sup}	total volume supplied by the pump station
$V_{\text{act}}^{(s)}$	effective fluid volume delivered to the actuators
$J_l^{(s)}$	fluid-supply loss index under scenario s
$J_{i,\text{norm}}^{(s)}$	normalized value of sub-objective i
$J_i^{\min}$	minimum value used for min–max normalization
$J_i^{\max}$	maximum value used for min–max normalization
$J_{\text{rob}}(X)$	robust objective function averaged over all optimization scenarios
k_{p}	pump flow coefficient
$Q_{\min}$	minimum pump-station flow rate
$Q_{\max}$	maximum pump-station flow rate
N_{pop}	genetic algorithm population size
N_{gen}	maximum number of generations
ε_u	maximum allowable unmet-flow ratio
MAE	mean absolute error

RMSE root-mean-square error

References

1. Wang, G.; Xu, Y.; Ren, H. Intelligent and Ecological Coal Mining as Well as Clean Utilization Technology in China: Review and Prospects. *Int. J. Min. Sci. Technol.* **2019**, *29*, 161–169. [CrossRef]
2. Ralston, J.C.; Reid, D.C.; Dunn, M.T.; Hainsworth, D.W. Longwall Automation: Delivering Enabling Technology to Achieve Safer and More Productive Underground Mining. *Int. J. Min. Sci. Technol.* **2015**, *25*, 865–876. [CrossRef]
3. Li, M.; Qi, Y.; Wang, W.; Li, Y.; Fu, Z.; Liu, Q.; Liu, S. Trajectory Tracking Control of the Hydraulic Servo System Subject to Random Impulsive Disturbances. *AIMS Math.* **2026**, *11*, 14323–14340. [CrossRef]
4. Mei, Z.; Wang, X.; Xie, J.; Li, S.; Liu, J. A Sensing System and Solving Method for Dynamic Detection of Relative Pose of Hydraulic Support Group. *Measurement* **2025**, *243*, 116145. [CrossRef]
5. Zeng, Q.; Jia, B.; Zhao, J.; Lv, Y.; Wan, L.; Meng, Z. Adaptive Learning Based Optimal Prescribed Performance Tracking Error Measurement of Hydraulic Support Initial Support Force. *IEEE Trans. Instrum. Meas.* **2025**, *74*, 1–14. [CrossRef]
6. Yang, S.; Yue, H.; Li, Q.; Chen, Y. Study on Failure Behaviors of Roofs with Varying Thicknesses in Longwall Coal Mining Working Face. *Rock Mech. Rock Eng.* **2024**, *57*, 6259–6282. [CrossRef]
7. Ding, H.; Li, Y.; Zhu, Q.; Su, J. Position Servo with Variable Speed Pump-Controlled Cylinder: Design, Modelling and Experimental Investigation. *Int. J. Hydromechatronics* **2024**, *7*, 155–175. [CrossRef]
8. Zeng, X.; Wang, D. Optimal Tracking Control of the Coal Mining Face Fluid Supply System via Adaptive Dynamic Programming. *Sci. Rep.* **2023**, *13*, 20002. [CrossRef] [PubMed]
9. Cao, C.; Gao, K.; Wang, H.; Pan, Y.; Deng, Z.; Xu, H.; Huang, D.; Zhao, X.; Zhao, J. Hydraulic Support Liquid Supply System Adaptive Pump Controlled Pressure Stabilization Control Under Strong Time-Varying Load. *Processes* **2024**, *12*, 2774. [CrossRef]
10. Cao, C.; Deng, Z.; Liu, H.; Wang, H.; Gao, K.; Pan, Y.; Huang, D.; Han, J.; Zhao, J. Study on Impact Characteristics of Turbulent Pipeline in High-Pressure and Large-Flow Long Distance Liquid Supply System. *IEEE/ASME Trans. Mechatron.* **2026**, 1–11. [CrossRef]
11. Tan, C.; Qi, N.; Zhou, X.; Liu, X.; Yao, X.; Wang, Z.; Si, L. A Pressure Control Method for Emulsion Pump Station Based on Elman Neural Network. *Comput. Intell. Neurosci.* **2015**, *2015*, 684096. [CrossRef] [PubMed]
12. Zhang, C.; Zhao, S.H.; Guo, G.; Dong, W.K. Modeling and Simulation of Emulsion Pump Station Pressure Control System Based on Electro-Hydraulic Proportional Relief Valve. *Appl. Mech. Mater.* **2012**, *190*, 860–864.
13. Peng, Y.; Kou, Z.; Wu, J.; Luo, J.; Liu, H.; Zhang, B. Research on a Pressure Control Method for a Liquid Supply System Based on Online Updating of a Radial Basis Function Neural Network. *Processes* **2023**, *12*, 57. [CrossRef]
14. Hou, T.; Shi, C.; Kou, Z.; Wu, J.; Zhang, B.; Peng, Y. Research on Positioning Control Strategy of Hydraulic Support Pushing System Based on Multistage Speed Control Valve. *Sci. Rep.* **2024**, *14*, 19046. [CrossRef] [PubMed]
15. Wang, B.; Zhao, X.; Quan, L.; Li, Y.; Hao, Y.; Ge, L. A Method for Improving Flow Control Valve Performance Based on Active Differential Pressure Regulation. *Measurement* **2023**, *219*, 113271. [CrossRef]
16. Liao, Y.; Zhao, W.; Feng, J.; Lian, Z. Optimization of the Control Performance of a Novel 3/2 Water Proportional Directional Valve with a Special Position Following Servo Mechanism. *IEEE/ASME Trans. Mechatron.* **2024**, *29*, 3391–3400. [CrossRef]
17. Li, M.Z.; Niu, Y.Q.; Xin, J.X.; Wang, C.Y. Effect Research of Leg Arrangement Mode for Mechanics Analysis of 2-Legs Shield Powered Support. *Adv. Mater. Res.* **2013**, *619*, 218–224.
18. Calafiore, G.C.; Campi, M.C. The Scenario Approach to Robust Control Design. *IEEE Trans. Autom. Contr.* **2006**, *51*, 742–753. [CrossRef]
19. Care, A.; Garatti, S.; Campi, M.C. Scenario Min-Max Optimization and the Risk of Empirical Costs. *SIAM J. Optim.* **2015**, *25*, 2061–2080. [CrossRef]
20. Garatti, S.; Campi, M.C. Non-Convex Scenario Optimization. *Math. Program.* **2025**, *209*, 557–608. [CrossRef]
21. Wang, X.; Song, X.; Sun, W. Surrogate Based Trajectory Planning Method for an Unmanned Electric Shovel. *Mech. Mach. Theory* **2021**, *158*, 104230. [CrossRef]
22. Fu, T.; Hu, Z.; Song, X.; Li, G.; Yue, H. Surrogate-Based Excavation Trajectory Generation of Unmanned Excavator under Uncertainty. *Appl. Math. Model.* **2025**, *148*, 116235. [CrossRef]
23. Mercy, T.; Jacquod, N.; Herzog, R.; Pipeleers, G. Spline-Based Trajectory Generation for CNC Machines. *IEEE Trans. Ind. Electron.* **2019**, *66*, 6098–6107. [CrossRef]
24. Simba, K.R.; Uchiyama, N.; Sano, S. Real-Time Smooth Trajectory Generation for Nonholonomic Mobile Robots Using Bézier Curves. *Robot. Comput. Integr. Manuf.* **2016**, *41*, 31–42. [CrossRef]
25. Biagiotti, L.; Melchiorri, C. Optimization of Generalized S-Curve Trajectories for Residual Vibration Suppression and Compliance with Kinematic Bounds. *IEEE/ASME Trans. Mechatron.* **2020**, *26*, 2724–2734. [CrossRef]

26. Van Hoek, R.; Ploeg, J.; Nijmeijer, H. Cooperative Driving of Automated Vehicles Using B-Splines for Trajectory Planning. *IEEE Trans. Intell. Veh.* **2021**, *6*, 594–604. [CrossRef]
27. Li, F.; Shang, Z.; Liu, Y.; Shen, H.; Jin, Y. Inverse Distance Weighting and Radial Basis Function Based Surrogate Model for High-Dimensional Expensive Multi-Objective Optimization. *Appl. Soft Comput.* **2024**, *152*, 111194. [CrossRef]
28. Bai, J.; Liu, G.-R.; Rabczuk, T.; Wang, Y.; Feng, X.-Q.; Gu, Y. A Robust Radial Point Interpolation Method Empowered with Neural Network Solvers (RPIM-NNS) for Nonlinear Solid Mechanics. *Comput. Methods Appl. Mech. Eng.* **2024**, *429*, 117159. [CrossRef]
29. Vergamini, E.G.; Zanette, C.; Maitan, L.; dos Santos, L.F.; Nostrani, M.P.; Boaventura, T. Quantitative Analyses of the Influence of Practical Aspects on Hydraulic Force Control Performance. *Int. J. Hydromechatronics* **2025**, *8*, 359–386. [CrossRef]

Disclaimer/Publisher's Note: The statements, opinions and data contained in all publications are solely those of the individual author(s) and contributor(s) and not of MDPI and/or the editor(s). MDPI and/or the editor(s) disclaim responsibility for any injury to people or property resulting from any ideas, methods, instructions or products referred to in the content.